

Supplemental material: Microphase separation in oil-water mixtures containing hydrophilic and hydrophobic ions

Nikos Tasios,¹ Sela Samin,² René van Roij,² and Marjolein Dijkstra¹

¹*Soft Condensed Matter, Debye Institute for Nanomaterials Science, Utrecht University, Princetonplein 1, 3584 CC, Utrecht, The Netherlands*

²*Institute for Theoretical Physics, Center for Extreme Matter and Emergent Phenomena, Utrecht University, Princetonplein 5, 3584 CC Utrecht, The Netherlands*

I. MAGGS'S METHOD

According to Maggs's method [1, 2], in a Monte Carlo simulation, the electrostatics can be simulated by generating configurations with a probability proportional to the Boltzmann distribution with the following Hamiltonian for the electrostatic energy,

$$\mathcal{H}_D = \frac{1}{2} \int d\mathbf{r} \frac{\mathbf{D}^2(\mathbf{r})}{\varepsilon(\mathbf{r})}, \quad (\text{S1})$$

where $\varepsilon(\mathbf{r})$ is the spatially varying dielectric, and $\mathbf{D}(\mathbf{r})$ is the electric displacement field, which obeys Gauss's law,

$$\nabla \cdot \mathbf{D}(\mathbf{r}) - \rho(\mathbf{r}) = 0, \quad (\text{S2})$$

with $\rho(\mathbf{r})$ the charge density field. For brevity's sake we shall drop the explicit dependence on the variable \mathbf{r} . We can then write the partition function by taking the path integral over all configurations of the electric displacement and charge density fields.

$$\mathcal{Z} = \int \mathcal{D}\rho \int \mathcal{D}\mathbf{D} \delta[\nabla \cdot \mathbf{D} - \rho] e^{-\frac{\beta}{2} \int d\mathbf{r} \frac{\rho^2}{\varepsilon}}. \quad (\text{S3})$$

The general solution to Gauss's law eq. (S3), is given by $\mathbf{D} = \mathbf{D}_{\parallel} + \mathbf{D}_{\perp}$, with $\mathbf{D}_{\parallel} = -\varepsilon \nabla \phi$ and $\mathbf{D}_{\perp} = \nabla \times \mathbf{Q}$ being the longitudinal and transverse parts, respectively. By doing so, the partition function factorizes,

$$\begin{aligned} \mathcal{Z} &= \int \mathcal{D}\rho e^{-\frac{\beta}{2} \int d\mathbf{r} \varepsilon (\nabla \phi)^2} \\ &\times \int \mathcal{D}\mathbf{D}_{\perp} \delta[\nabla \cdot \mathbf{D}_{\perp}] e^{-\frac{\beta}{2} \int d\mathbf{r} \frac{\mathbf{D}_{\perp}^2}{\varepsilon}} \\ &= \mathcal{Z}_{\text{Coulomb}} \times \mathcal{Z}_{\perp}. \end{aligned} \quad (\text{S4})$$

Here, \mathcal{Z}_{\perp} is independent of the charge positions and depends only on the solvent sites through the local dielectric constant, since it contains only integrations over the transverse field degrees of freedom. Therefore, \mathcal{Z}_{\perp} is responsible for the shift in the phase diagram of the solvent mixture when the polar nature of the solvents is included. In Eq. (S4), $\mathcal{Z}_{\text{Coulomb}}$ gives the Coulomb interactions between the charged particles. From the above, it is evident that only the transverse degrees of freedom need to be integrated out, along with the charge positions with the restriction that Gauss's law is preserved. The system is subsequently discretized by defining a lattice of $N = N_x N_y N_z$ sites with periodic boundary conditions.

The electric field is discretized on the links between the lattice sites. This discretization scheme is often also used when solving Poisson's equation using finite difference methods [3] (see also figure S1). We denote the field on the link between sites i and j as D_{ij} .

II. DIELECTRIC INTERPOLATION AT LATTICE LINKS

To make the species in our model polar, we assign a dielectric permittivity ε_{μ} to each lattice site. For Maggs's method, however, knowledge of the value of the dielectric constant at the positions of the lattice *links* is required. We choose to interpolate the dielectric permittivity on the link between sites i and j by taking the harmonic mean of the permittivities of the two sites as follows [4],

$$\frac{1}{\varepsilon_{ij}} = \frac{1}{2} \left(\frac{1}{\varepsilon_i} + \frac{1}{\varepsilon_j} \right), \quad (\text{S5})$$

where $\varepsilon_i = \sum_{\mu} \varepsilon_{\mu} o_{i\mu}$ is the dielectric permittivity of the species occupying site i . This is similar to Yee's finite-difference time-domain scheme, where effective permittivities are used to account for offsets of dielectric interfaces from grid nodes [5]. Note that we can also write $1/\varepsilon_i = \sum_{\mu} (1/\varepsilon_{\mu}) o_{i\mu}$, which leads to the following expression for the dielectric permittivity of link $\{i, j\}$,

$$\frac{1}{\varepsilon_{ij}} = \sum_{\mu} \frac{1}{2\varepsilon_{\mu}} (o_{i\mu} + o_{j\mu}). \quad (\text{S6})$$

III. SIMULATION DETAILS

The solvent and ions in our lattice model are simulated in the canonical ensemble using the following Monte Carlo moves:

1. Attempt to translate a solvent site by swapping it with a nearest-neighbour solvent site of the opposite species.
2. Attempt to swap an ion site with a nearest-neighbour solvent site.
3. Attempt to modify the circulation of the displacement field D in a closed directed loop.

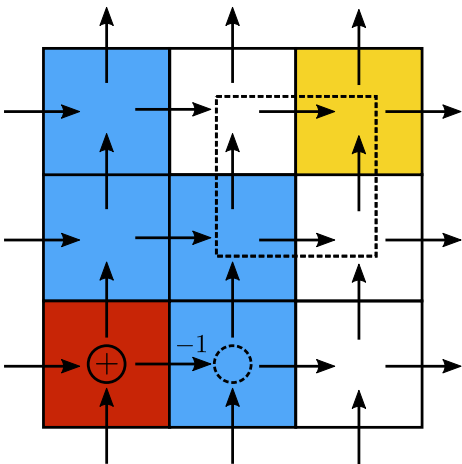


FIG. S1. Schematic representation of the lattice model of an ion-solvent mixture with the grid representing the lattice sites. The different colors represent the different species of the model, with white and blue representing A and B solvent species, respectively, and yellow and red representing negative and positive ions. The arrows represent the discretized electric field of Maggs’s method – the magnitude of the field is not shown here. The dotted square encloses a field plaquette. In the lower left corner, a positive ion is drawn. To move the ion to the lattice site to the right, the reduced D field on the link between the two sites needs to be modified by -1 , such that Gauss’s law is satisfied.

4. Attempt to modify the global field D_g to impose metallic boundary conditions [6].

These moves are accepted/rejected using the standard Metropolis acceptance criterion, $a = \min[1, \exp(-\beta\Delta\mathcal{H})]$, where the energy difference, $\Delta\mathcal{H}$, is calculated from Eq. (1) of the main text. Sites in move 1 are chosen randomly from the lattice, and moves which end up picking a non-solvent site are immediately rejected. For the ion translations in move 2, we keep a list of their positions, so we can randomly pick an ion straightforwardly. In each Monte Carlo cycle, we perform moves 1 and 3 N times, move 2 N_{\pm} times, and move 4 once.

To simulate the solvent grand-canonically, step 1 is replaced by an attempt to ‘flip’ the species of a solvent site, and is accepted by the Metropolis criterion,

$$a(N_B \rightarrow N_B \pm 1) = \min \left[1, e^{-\beta(\Delta\mathcal{H} \mp \epsilon\Delta\mu_s)} \right], \quad (\text{S7})$$

where $\Delta\mu_s = (\mu_B - \mu_A)/\epsilon$ is the chemical potential difference between the solvent species.

When we move an ion from site i to its neighbour site j , in the case of move 2, the field on the link connecting sites i and j , D_{ij} , needs to be modified by $-(o_{i+} - o_{i-})$ to satisfy Gauss’s law, see Fig. S1. The move is then accepted with the standard Metropolis criterion, based on the change in electrostatic energy, given by the second part in Eq. (1) of the main text. Additionally, to increase the acceptance rate, we use temporary charge spreading,

as described in Ref. [7], and later generalized by Maggs *et al.* [4]. The concept of temporary charge spreading is simple; the charge of the ion is temporarily spread to neighbouring sites according to some rule that maximizes the overall acceptance, they are subsequently translated, and pulled back in. The benefit of temporary spreading is that the modification of the electric field is also spread out, leading to an overall higher acceptance based on the spreading range.

To generate configurations of the displacement field D with the correct statistical weight, an additional Monte Carlo move is introduced (move 3 above), which integrates over the transverse degrees of freedom, D_{\perp} , by modifying the field circulation. This can be achieved by modifying the field along a closed directed path, by some random value, and again, accepted based on the energy change in Eq. (1) of the main text. The simplest path satisfying the above requirements is shown in Fig. S1, and is commonly referred to as a plaquette. As described in Refs. [2, 6], under periodic boundary conditions, the displacement field decomposes into

$$D = -\epsilon\nabla\phi + \nabla \times Q + D_g, \quad (\text{S8})$$

where the global displacement field $D_g = \text{const}$, and ϕ is the electrostatic potential. Tinfoil boundary conditions set the dielectric constant at infinite distance to $\epsilon_{\infty} = \infty$, while the vacuum boundary conditions set it to $\epsilon_{\infty} = 1$. If we wish to simulate tinfoil, instead of vacuum boundary conditions, D_g also needs to be relaxed via a Monte Carlo move (move 4 above).

Before the start of the simulation, the electric field should be initialized, such that it is consistent with Gauss’s law. A simple procedure is to initialize the electric field to zero, and then take a Hamiltonian path through the lattice, e.g., a path that visits each site exactly once, and solve Gauss’s law for each site visited by modifying the link to the next site in the path. On arriving at site p_i , i.e., the i -th step of the path p , holding a charge $q_{p_i} = o_{p_i+} - o_{p_i-}$, we have already solved the Gauss constraint for sites $\{p_1, \dots, p_{i-1}\}$. The incoming link to the site, $\{p_{i-1}, p_i\}$, thus bears the initialized field $D_{p_{i-1}, p_i} = \sum_{j=1}^{i-1} q_{p_j}$. The outgoing field $D_{p_i, p_{i+1}}$ is then set to $\sum_{j=1}^{i-1} q_{p_j}$, so that $D_{p_i, p_{i-1}} + D_{p_i, p_{i+1}} = q_{p_i}$. Gauss law is now fulfilled on site p_i , and we proceed to site p_{i+1} . At the end of the path, we reach site p_N with $D_{p_{N-1}, p_N} = \sum_{j=1}^{N-1} q_{p_j}$. Imposing periodic boundary conditions in charged systems is only possible if the total charge Q is zero (otherwise the total energy is divergent). Thus, $D_{p_{N-1}, p_N} = Q - q_{p_N} = -q_{p_N}$, and Gauss law is satisfied everywhere on the lattice.

IV. MEAN FIELD THEORY

From our observations in Fig. 4(a), we can build a simple mean-field model. As a first approximation, we assume that both ionic species and the solvent species, partition completely between the two lamella regions, and

that their densities are position independent within the regions. We denote the salt concentration, $c = N_{\pm}/N$, the dimensionless surface area of an AB lamella as A , and the dimensionless thickness as δ , with the thickness of the A -rich lamellae being $x_A\delta$, and that of B -rich lamellae, $x_B\delta$. The number of AB lamellae k in a box of reduced length L is given by $k = L/\delta$. Note that $N = LA$. With these assumptions and definitions, we can write an expression for the free energy of the ions in the system,

$$\begin{aligned} \frac{F_{\text{lam}}}{\epsilon N} &= \frac{x_A c_+^A}{\beta} \ln c_+^A + \frac{x_B c_-^B}{\beta} \ln c_-^B \\ &\quad - \frac{3c(1-c)}{2x_B} J_{B+} + \frac{2k\gamma A}{N} \\ &\quad + \frac{\Gamma A k}{2N} \left[\int_{-\delta x_A/2}^{\delta x_A/2} ds D_A^2(r) + \int_{-\delta x_B/2}^{\delta x_B/2} ds \frac{D_B^2(r)}{\epsilon_B^*} \right]. \end{aligned} \quad (\text{S9})$$

The first two terms in Eq. (S9) correspond to the entropy of the ions, with $\beta = \epsilon/(k_B T)$. Here, the concentration of positive ions in the A -rich phase is $c_+^A = N_+/N_A = (N_{\pm}/2)/(x_A N) = c/2x_A$, and that of the negative ions in the B -rich phase is $c_-^B = c/2x_B$. The third term in Eq. (S9) is the solvation energy of the ions. An energy penalty is paid for the formation of the $2k$ interfaces, which is seen in the fourth term, where γ is the dimensionless surface tension. The last term in Eq. (S9) is the electrostatic energy, with the integration performed in the lamella-normal direction s . The displacement field inside the A/B lamella can be calculated from symmetry considerations: $D_{A/B}(r) = cs/2x_{A/B}$. Using this in Eq. (S9), we arrive at

$$\begin{aligned} \frac{F_{\text{lam}}}{\epsilon N} &= \frac{c}{\beta} \ln c - \frac{c}{2\beta} \ln [4x_B(1-x_B)] - \frac{3(1-c)c}{2x_B} J_{B+} \\ &\quad + \frac{2\gamma}{\delta} + \frac{\Gamma c^2 \delta^2}{192} \left[(1-x_B) + \frac{x_B}{\epsilon_B^*} \right]. \end{aligned} \quad (\text{S10})$$

The free energy of the ions in the phase separated state, assuming again that the ions partition completely, is given by

$$F_{AB}/\epsilon N = \frac{c}{\beta} \ln \frac{c}{2} + \frac{2\gamma}{L} - 3(1-c)c/x_B, \quad (\text{S11})$$

which leads to the following free-energy difference between the two phases,

$$\begin{aligned} \frac{\Delta F_{\text{lam}}}{\epsilon N} &= \frac{F_{\text{lam}} - F_{AB}}{\epsilon 3N} = \frac{c}{\beta} \ln 2 - \frac{c}{2\beta} \ln [4x_B(1-x_B)] \\ &\quad - \frac{3(1-c)c}{2x_B} (J_{B+} - 1) \\ &\quad + 2\gamma \left(\frac{1}{\delta} - \frac{1}{L} \right) + \frac{\Gamma c^2 \delta^2}{192} \left[\frac{1-x_B}{\epsilon_A} + \frac{x_B}{\epsilon_B} \right]. \end{aligned} \quad (\text{S12})$$

Minimizing ΔF_{lam} with respect to the lamella thickness δ , we arrive at Eq. (2) of the main text.

To evaluate Eq. (2) of the main text, we need to calculate the surface tension. This is done using the results for the probability density $P(x_B)$, from the TMMC simulations of the pure solvent mixture as [8],

$$\gamma = \frac{1}{2L^2\beta} \Delta P, \quad (\text{S13})$$

where

$$\begin{aligned} \Delta P &= \frac{1}{2} \left(\max_{x_B < x_B^{\text{min}}} \ln P(x_B) + \max_{x_B > x_B^{\text{min}}} \ln P(x_B) \right) \\ &\quad - \ln P(x_B^{\text{min}}), \end{aligned} \quad (\text{S14})$$

and x_B^{min} is the position at which the probability distribution $P(x_B)$ is minimized. The first term amounts to an average over the two maxima of $\ln P(x_B)$.

V. STRUCTURE FACTORS

The static partial structure factors $S_{\mu\nu}(\mathbf{k})$ for a multi-component system are defined [9] as

$$S_{\mu\nu}(\mathbf{k}) = \left\langle \frac{1}{N} \rho_{\mu}(\mathbf{k}) \rho_{\nu}(-\mathbf{k}) \right\rangle, \quad (\text{S15})$$

via the Fourier components of the species densities. For a lattice, this can be written as

$$\rho_{\mu}(\mathbf{k}) = \sum_{i=0}^N o_{i\mu} e^{-i\mathbf{k}\cdot\mathbf{r}_i} \quad (\text{S16})$$

which is the discrete Fourier transform of the occupancy of species μ . With this definition it is easy to calculate $S_{\mu\nu}(\mathbf{k})$ efficiently, directly from Eq. (S15), with the aid of the fast Fourier transform [10].

In Fig. S2 and Fig. S3, we plot the partial structure factors for solvent B, $S_{BB}(k)$, as a function of the dimensionless wavevector k . In Fig. S2 the structure factors are plotted for a temperature $\tau = -0.2$. We find a peak in the structure factor, which shifts to lower values of k as x_B is increased, see also Fig. 4(b) of the main text. This corresponds to increasingly longer-ranged correlations, leading up to the lamellar phase, where solvent species between lamellae are highly correlated. Some correlations appear also at larger wavevectors, corresponding to correlations also between ‘‘second-neighbour’’ lamellae. With the exception of the lamellar phase, we find it hard to distinguish between the different phases from the structure factor plots alone. In Fig. S3, we plot $S_{BB}(k)$ for $\tau \in [-0.3, 0.1]$ at $x_B = 0.5$. Here, we find that the position of the small k peak changes significantly only for the highest temperature. Moreover, the layers in the bicontinuous disordered phase (labeled D, see representative images in Fig. S4) have a size almost equal to that of the lamellae in the lamellar phase. These results underline the possibility that in the experimental set-ups used thus far [11], one would be unable to detect the rich mesophase behavior we find by examining scattering experiments results.

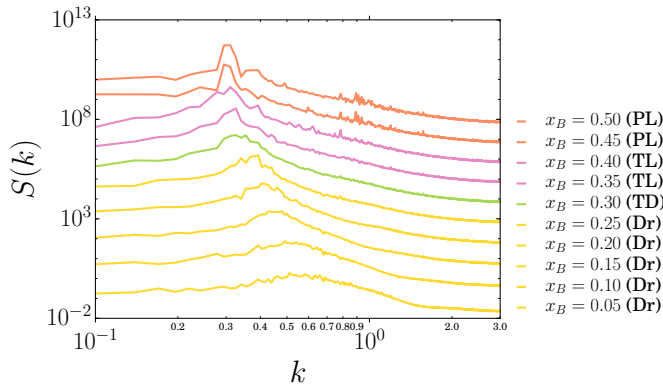


FIG. S2. Radially averaged partial structure factor, $S_{BB}(k)$, as a function of the dimensionless wavevector, k , for $x_B \in [0.05, 0.5]$ and at $\tau = -0.2$. The labels in the legend denote the corresponding phase at the different x_B . The colors are based on the colors given for the different phases in the phase diagram in Fig. 2 of the main text.

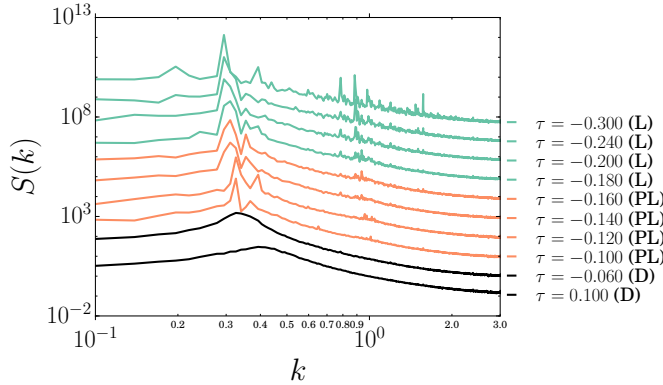


FIG. S3. $S_{BB}(k)$ for $\tau \in [-0.3, 0.1]$ at $x_B = 0.5$. Here also, the colors are based on the colors scheme of Fig. 2 of the main text, with the exception of the black, which denotes the bicontinuous disordered phase.

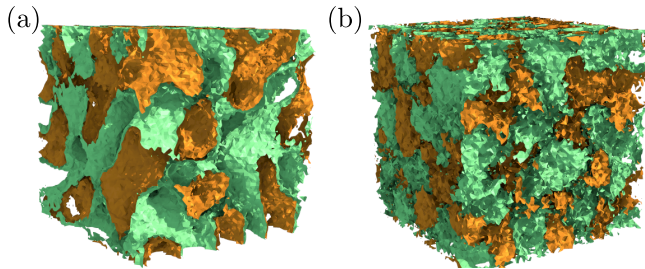


FIG. S4. Representative x_B iso-composition surfaces of the bicontinuous disordered phase at high temperature. The orange/green surface represents the side of the B/A (minority/majority) phase. Here, $x_B = 0.5$ and $\tau = 0$ in (a), while $\tau = 0.1$ in (b). The smaller domain size and the effect of thermal noise are clearly observed at the higher temperature.

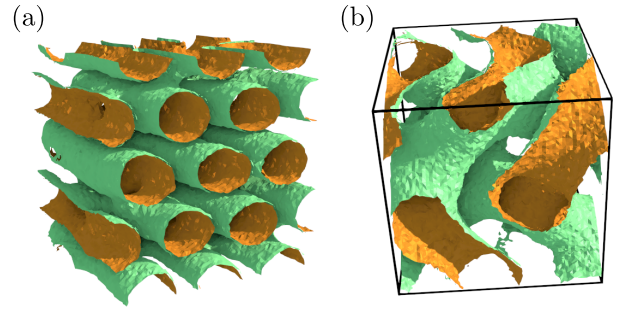


FIG. S5. Representative x_B iso-composition surfaces of two observed mesophases at $\varepsilon_B^* = 9$. The orange/green surface represents the side of the B/A (minority/majority) phase. We show a hexagonally ordered tubular phase in (a), and a gyroid phase in (b).

VI. PRELIMINARY RESULTS FOR LARGE DIELECTRIC CONTRAST

Given the large parameter space of our model, we explored only a small fraction here. Preliminary results using, e.g., a higher dielectric contrast $\varepsilon_B^* = 9$, seem to confirm the existence of additional phases, also seen in diblock copolymer systems, such as the gyroid phase, and hexagonally ordered droplet and tubular phases. Representative isosurfaces of a gyroid phase and a hexagonally ordered tubular phase are shown in S5.

-
- [1] A. C. Maggs and V. Rossetto, *Physical Review Letters* **88**, 196402 (2002).
- [2] A. C. Maggs, *The Journal of chemical physics* **120**, 3108 (2004).
- [3] K. S. Yee *et al.*, *IEEE Trans. Antennas Propag* **14**, 302 (1966).
- [4] L. Levrel and A. C. Maggs, *Physical Review E* **72**, 016715 (2005).
- [5] T. Hirono, Y. Shibata, W. Lui, S. Seki, and Y. Yoshikuni, *IEEE microwave and guided wave letters* **10**, 359 (2000).
- [6] L. Levrel and A. C. Maggs, *The Journal of chemical physics* **128**, 214103 (2008).
- [7] A. Duncan, R. Sedgewick, and R. Coalson, *Physical Review E* **71**, 046702 (2005).
- [8] J. R. Errington, *Phys. Rev. E* **67**, 012102 (2003).
- [9] J. Hansen and I. McDonald, *Theory of Simple Liquids* (Elsevier Science, 2006).
- [10] M. E. J. Newman and G. T. Barkema, *Monte Carlo methods in statistical physics* (Clarendon Press; Oxford University Press, New York, 1999).
- [11] K. Sadakane, M. Nagao, H. Endo, and H. Seto, *The Journal of chemical physics* **139**, 234905 (2013).